Simulation Modelling Practice and Theory 16 (2008) 1503–1513

Contents lists available at ScienceDirect

Simulation Modelling Practice and Theory

journal homepage: www.elsevier.com/locate/simpat

Dynamic eccentricity in squirrel cage induction motors – Simulation and analytical study of its spectral signatures on stator currents

M. Sahraoui *, A. Ghoggal, S.E. Zouzou, M.E. Benbouzid

Laboratoire de Génie Electrique de Biskra (LGEB), University of Biskra, BP145 Biskra, Algeria

ARTICLE INFO

Article history:
Received 15 May 2008
Received in revised form 10 August 2008
Accepted 12 August 2008
Available online 20 August 2008

Keywords:
Diagnosis
Induction motors
Dynamic eccentricity
Principal slot harmonics
Flux density
Airgap permeance

ABSTRACT

Most of faults in three-phase induction motors have relationship with airgap eccentricity. There are two forms of airgap eccentricity: static (SE) and dynamic (DE). According to the literatures, the well known signatures of dynamic eccentricity, on the stator current spectra, are sidebands around the principal slot harmonics (PSH). However, many other researches have shown that DE induces also spectral components around the fundamental, but few are reported on the sources and the causes of these components. In this direction and since it is difficult to study experimentally the DE separately from the SE; the present paper attempts to explain, analytically and by simulation, the generation process of all frequency components that are a function of only DE. For that reason, a detailed analytical study for three-phase induction motors working under DE is performed. This study is based on rotating field approach. A general theoretical analysis of the interaction between all harmonics of the eccentric airgap permeance and the stator and rotor MMF components is put forward. The simulation results, obtained from an accurate model, confirm the existence of specific frequency components around the fundamental, caused by the dynamic airgap eccentricity. The interactions between the DE and the inherent SE are also illustrated using this mathematical model.

1. Introduction

The three-phase squirrel cage induction motors are the most common prime machines in industrial processes. This is chiefly due to their low cost, reasonable size, ruggedness and low maintenance. Usually, the induction motors work under many stresses from various nature (thermal, electric, mechanical and environment) which can affect their lifespan by involving the occurrence of stator and/or rotor faults [1,2,7,35]. The need for on-line condition monitoring of large induction motors has increased because a sudden failure of critical motor can cause great economical losses. Therefore, the main goal of the operator of electrical drives is to reduce the maintenance costs and to prevent unscheduled downtime of these machines.

Machine eccentricity is the condition of the unequal airgap that exist between the stator and rotor [1,10–12,18,22,33]. An induction machine can fail due to airgap eccentricity. This fault can result from variety of sources such as incorrect bearing positioning during assembly, worn bearings, a shaft deflection, and so on. There are two forms of airgap eccentricity: static eccentricity (where the rotor is displaced from the stator bore centre but is still turning upon its own axis) and dynamic eccentricity (where the rotor is still turning upon the stator bore centre but not on its own centre).

Through the literatures, one can found a lot of techniques used to detect airgap eccentricity. Some techniques are based on the spectral analysis of some signals sensing from the induction motors, such as the stator core vibration [3,4], airgap and axial flux [5], instantaneous power [6] and current Park's vector [19]. Other techniques can be found in [8,23,26,27,29,30].

* Corresponding author. Tel./fax: +213 33734985.
E-mail address: s_moh78@yahoo.fr (M. Sahraoui).

1569-190X/$ - see front matter © 2008 Elsevier B.V. All rights reserved.
doi:10.1016/j.simpat.2008.08.007

The preferred method, used in industry, to diagnose stator and rotor faults in induction motors is the MCSA [7–11,31–34]. This technique is based on the monitoring of stator current spectra. The appearance of new harmonics or increase in magnitude of some other at specific frequencies indicates a fault in the machine. So, the signal given by current sensors must be correctly analysed in both healthy and faulty conditions.

There have been a number of papers dealing the effect of airgap eccentricity on the airgap flux density and on the stator currents. Using MCSA, the sideband frequencies associated with an eccentricity are [9–12]

$$f_1 = \left[(kN_r \pm n_d)\frac{(1-s)}{p} \pm v\right] f_s \tag{1}$$

where k is any positive integer, N_r is the number of rotor slots, $n_d = 0$ in case of static eccentricity and $n_d = 1, 2, \ldots$ in case of dynamic eccentricity (it is known as dynamic eccentricity order), s is the slip, p is the number of pole-pairs, f_s is the fundamental supply frequency and $v = 1, 3, 5, \ldots$ is the order of the stator time harmonics that are present in the power supply. Furthermore, if both static and dynamic eccentricities exist together, spectral components can be observed around the fundamental, which are given by [1,3,10,12,14,20]

$$f_{\text{mix}} = f_s \pm m f_r \tag{2}$$

with $m = 1, 2, 3, \ldots$ and $f_r = (1 - s) f_s/p$ the mechanical rotational frequency.

The expression (1) is derived from the MMF-permeance wave approach and it shows that DE induces sidebands around the rotor slot harmonics (RSH) while the SE can not produce any new components in the stator current spectra; but it causes only an increase in the magnitudes of the RSH. However, experimental results from laboratory work and industrial case histories [11] show that it was inconclusive to identify static or dynamic eccentricity using expression (1), since a high SE also produced DE components [17,28]. On the other hand, exploratory tests have shown that DE induces harmonics at $(f_s \pm f_r)$ Hz in the stator current spectra (like the mixed eccentricity) [11] which, by the classical MMF-permeance wave analysis, should not be present [3,13]. These experimental observations are also confirmed in many other works [1,8,17,21,25] but few are reported on the generation process of these components. So, one can note some ambiguities, between the signatures of the DE and the mixed eccentricity, and these need more explanation and clarification.

For that reason and since a reliable diagnosis requires a good understanding of fault mechanisms and its signatures, this paper attempts to explain the effect of dynamic eccentricity on the production of specific frequency components around the fundamental and the PSH. It is important to note that this study is mainly based on the research and results obtained by [15], which can be classed among the few works dealing this subject. The general form of the present study use the rotating field approach which considers the airgap flux density as a sum of harmonic fields obtained from the product of the airgap permeance and the stator and rotor MMFs. In summary, this analysis is based on the following description (Fig. 1):

The input is assumed to be three-phase sinusoidal supply; while the motor is assumed to have three-phase symmetrical stator windings. First, the stator main currents set up an MMF across the airgap. This MMF contains the fundamental and an infinite series of space harmonics which are due to the non sinusoidal spatial distribution of the stator windings. The airgap permeance consists of a constant term plus a series of harmonic components due to the eccentricity effects. This airgap per-

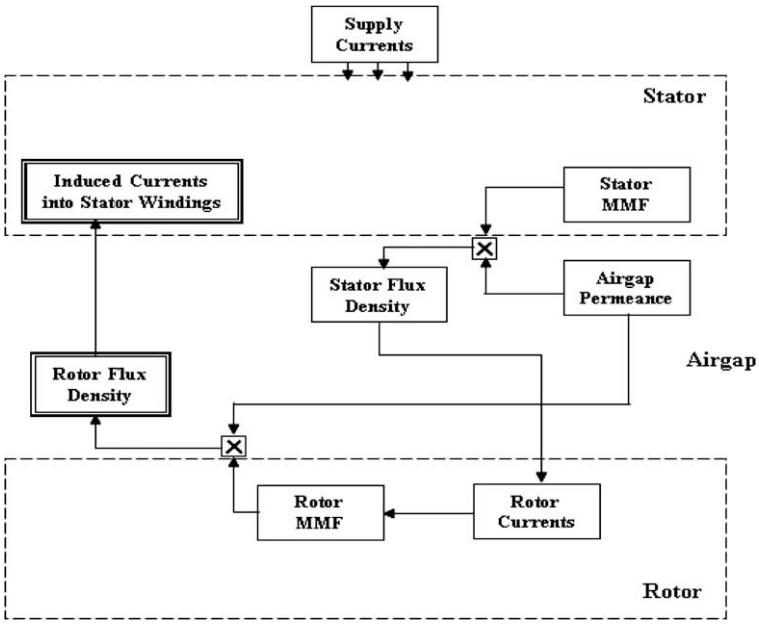

Fig. 1. Computation of the stator and rotor flux densities.

meance multiplied by the stator MMF produce the stator flux density with additional components. These stator flux density waves induce currents in the rotor bars which, in tern, give rise to a rotor MMF that contains supplementary terms due to the eccentricity fault. The interaction of this rotor MMF with the airgap permeance generates rotor flux density waves with further components due to the eccentric part of the airgap permeance. Depending on their number of pole-pairs, the new rotor flux density waves can induce corresponding current components in the stator windings.

2. Analytical study of healthy induction motor

2.1. The airgap flux density of symmetrical three-phase stator windings

It is well-known that the stator MMF of each phase is the product of the current and the winding function of this phase. Thus, for a symmetrical three-phase winding, one can write:

$$\begin{cases} F_{sA}(t,\theta) = \sum_n \widehat{F}_{An}[\sin(\omega_s t - np\theta) + \sin(\omega_s t + np\theta)] \\ F_{sB}(t,\theta) = \sum_n \widehat{F}_{Bn}\left[\sin\left(\omega_s t - \frac{2\pi}{3} - n\left(p\theta - \frac{2\pi}{3}\right)\right) + \sin\left(\omega_s t - \frac{2\pi}{3} + n\left(p\theta - \frac{2\pi}{3}\right)\right)\right] \\ F_{sC}(t,\theta) = \sum_n \widehat{F}_{cn}\left[\sin\left(w_s t - \frac{4\pi}{3} - n\left(p\theta - \frac{4\pi}{3}\right)\right) + \sin\left(w_s t - \frac{4\pi}{3} - n\left(p\theta - \frac{4\pi}{3}\right)\right)\right] \end{cases} \tag{3}$$

with $n = 2k + 1$ and $k = 0,1,2,3,\ldots$

The general term of the resulting stator MMF, can be written as

$$F_{sh}(t,\theta) = \widehat{F}_{sh}\sin(\omega_s t \pm hp\theta) \tag{4}$$

with, $\widehat{F}_{sh}$ the amplitude of the hth space harmonic and p is the number of pole-pairs. It was shown that the 3rd space harmonic and its multiples do not exist in the resulting stator MMF of balanced three-phase stator windings without neutral connection, thus: $h = 6k \pm 1$. However, these triplen space harmonics will be present, if the neuter line is connected or there is any unbalance in the stator windings; in such case: $h = 2k + 1$ with k an integer.

In the healthy state and neglecting the slots and saturation effects, the airgap permeance function is a constant:

$$P(t,\theta) = P_0 \tag{5}$$

The product of the stator MMF (4) with the airgap permeance (5) gives rise to the stator flux density which has the same waveform as the stator MMF. So, the general term of the stator flux density waves can be written as

$$B_{sh}^{P_0}(t,\theta) = \widehat{B}_{sh}^{P_0}\cos(\omega_s t \pm hp\theta) \tag{6}$$

where $\widehat{B}_{sh}^{P_0}$ is the amplitude of the hth stator flux density harmonic.

2.2. The rotor airgap flux density

A squirrel-cage rotor of N_r bars can be described as N_r identical and equally spaced loops. The hth stator flux density harmonic induces currents in the rotor loops with electrical pulsation of $s_h\omega_s$, where $s_h = 1 - h(1 - s)$ and s is the slip. Thus, the rotor loop currents can be written as

$$\begin{cases} I_{rh1}(t) = \widehat{I}_{rh}\cos(s_h\omega_s t) \\ I_{rh2}(t) = \widehat{I}_{rh}\cos\left(s_h\omega_s t - hp\frac{2\pi}{N_r}\right) \\ \cdots \\ I_{rhN_r}(t) = \widehat{I}_{rh}\cos\left(s_h\omega_s t - (N_r - 1)hp\frac{2\pi}{N_r}\right) \end{cases} \tag{7}$$

where $\widehat{I}_{rh}$ is the magnitude of the rotor loop currents induced by the hth stator flux density harmonic. Therefore, the rotor loop can be assumed as a one-turn coil ($w_r = 1$) with pitch equal to: $\alpha = 2\pi/N_r$. If the magnetic axes of the rotor loop1 is in the centre of the reference frame fixed to the rotor (Fig. 2); then, the distribution function of this loop can be written as

$$n_{rd\,loop1}(\theta_r) = \begin{cases} 1 & -\frac{\pi}{N_r} < \theta_r < +\frac{\pi}{N_r} \\ 0 & \text{otherwise} \end{cases} \tag{8}$$

Note that $n_{rd\ loop1}(\theta_r)$ is a periodic function. So, it can be resolved in Fourier series as follows:

$$n_{rd\,loop1}(\theta_r) = \frac{1}{N_r} + \sum_\eta \frac{2}{\eta\pi}\sin\left(\eta\frac{\pi}{N_r}\right)\cos(\eta\theta_r) \tag{9}$$

where $\eta = 1,2,3,\ldots$ is the order of the rotor space harmonics and it must be different from kN_r, with k an integer.

The winding function, of the first loop, is defined as

$$N_{rw}^{loop1}(\theta_r) = n_{rd\,loop1}(\theta_r) - \langle n_{rd\,loop1}(\theta_r)\rangle \tag{10}$$

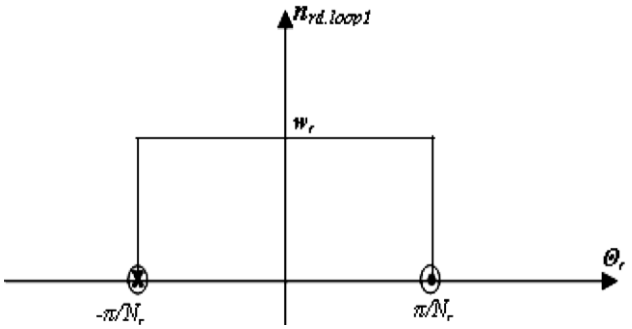

Fig. 2. Distribution function of the rotor loop 1.

where $\langle n_{rd\ loop1}(\theta_r)\rangle = 1/N_r$ is the mean value of the distribution function of the first loop. Since in general case, the induction motors have p pair of poles, the winding functions of the N_r rotor loops must be expressed in electrical degrees as follows:

$$\begin{cases} N_{rw}^{loop1}(\theta_r) = \sum\limits_{\eta=1} \frac{2}{\eta p\pi} \sin\left(\frac{\eta p\pi}{N_r}\right)\cos(\eta p\theta_r) \\ N_{rw}^{loop2}(\theta_r) = \sum\limits_{\eta=1} \frac{2}{\eta p\pi} \sin\left(\frac{\eta p\pi}{N_r}\right)\cos\left(\eta p\left(\theta_r - \frac{2\pi}{N_r}\right)\right) \\ \dots \\ N_{rw}^{loopN_r}(\theta_r) = \sum\limits_{\eta=1} \frac{2}{\eta p\pi} \sin\left(\frac{\eta p\pi}{N_r}\right)\cos\left(\eta p\left(\theta_r - (N_r-1)\frac{2\pi}{N_r}\right)\right) \end{cases} \tag{11}$$

Multiplying (7) by (11) leads to the MMF produced by each rotor loop (referenced to rotor):

$$\begin{cases} F_{rh}^{loop1}(t,\theta) = \sum\limits_{\eta=1} \widehat{F}\eta_{rh}\{\cos(s_h\omega_s t + \eta p\theta_r) + \cos(s_h\omega_s t - \eta p\theta_r)\} \\ F_{rh}^{loop2}(t,\theta_r) = \sum\limits_{\eta=1} \widehat{F}_{rh}^{\eta}\left\{\cos\left(s_h\omega_s t + \eta p\theta_r - (\eta+h)\frac{2\pi p}{N_r}\right) + \cos\left(s_h\omega_s t - \eta p\theta_r + (\eta-h)\frac{2\pi p}{N_r}\right)\right\} \\ \dots \\ F_{rh}^{loopN_r}(t,\theta_r) = \sum\limits_{\eta=1} \widehat{F}_{rh}^{\eta}\left\{\cos\left(s_h\omega_s t + \eta p\theta_r - (N_r-1)(\eta+h)\frac{2\pi p}{N_r}\right) + \cos\left(s_h\omega_s t - \eta p\theta_r + (N_r-1)(\eta-h)\frac{2\pi p}{N_r}\right)\right\} \end{cases} \tag{12}$$

The resulting MMF of the squirrel rotor cage is the sum of the MMFs of all rotor loops. Thus, one can obtain:

$$F_{rh}(t,\theta_r) = \sum_{i=1}^{N_r}\sum_{\eta=1} \widehat{F}_{rh}^{\eta}\left\{\cos\left(s_h\omega_s t + \eta p\theta_r - (i-1).(\eta+h)\frac{2\pi p}{N_r}\right) + \cos\left(s_h\omega_s t - \eta p\theta_r + (i-1)\cdot(\eta-h)\frac{2\pi p}{N_r}\right)\right\} \tag{13}$$

Expression (13) represents the sum of N_r waves shifted regularly in phase by $(\eta \pm h)2\pi p/N_r$. As a result, this sum is always null except three cases, when $\eta = \pm h$ as well as for $(\eta + h)p = kN_r$ and $(\eta - h)p = kN_r$. Note that η is a positive integer. Consequently, the cage rotor MMF waves exist only for:

$$\eta = \begin{cases} |h| \\ |\frac{kN_r}{p} \pm h| \end{cases} \tag{14}$$

It is so important to note that if the winding functions of the rotor loops (11) are expressed in mechanical degrees, we would have: $\eta = |hp|$ and $\eta = |kN_r \pm hp|$ which are not the order of the rotor space harmonics but the number of pole-pairs of these harmonics; and this leads to wrong results. Hence, one can state that each hth stator flux density harmonic produces rotor MMF harmonics with order numbers given by (14). The harmonics with orders equal to $(kN_r/p \pm h)$ are usually called rotor slot harmonics (RSH) which are the consequence of the space distribution of rotor bars. For $k = 1$ and $h = 1$, we obtain the well-known principle slot harmonics (PSH). So, with respect to the rotor, the general term of the squirrel rotor cage MMF can be written as

$$F_{rh}(t,\theta_r) = \widehat{F}_{rh1}\cos(s_h\omega_s t \pm hp\theta_r) + \widehat{F}_{rhSH1,2}\cos\left[s_h\omega_s t \pm \left(\frac{kN_r}{p} \mp h\right)p\theta_r\right] \tag{15}$$

To observe (15) from the stator side, we use the transformation given by

$$\theta_r = \theta - \frac{(1-s)}{p}\omega_s t \tag{16}$$

Thus, one can obtain:

$$F_{rh}(t,\theta) = \widehat{F}_{rh}\cos(\omega_s t \pm hp\theta) + \widehat{F}_{rhSH1,2}\cos\left[\left(1 \mp \tfrac{kN_r}{p}(1-s)\right)\omega_s t \pm \left(\tfrac{kN_r}{p} \mp h\right)p\theta\right] \quad (17)$$

In healthy state, the airgap permeance is a constant (5). As a result, the rotor flux density will have the same waveform (harmonics) as the rotor MMF. Hence, the general term of the rotor flux density can be written as

$$B_{rh}^{P_0}(t,\theta) = \widehat{B}_{rh}^{P_0}\cos(\omega_s t \pm hp\theta) + \widehat{B}_{rhSH1,2}^{P_0}\cos\left[\left(1 \mp \tfrac{kN_r}{p}(1-s)\right)\omega_s t \pm \left(\tfrac{kN_r}{p} \mp h\right)p\theta\right] \quad (18)$$

The rotor flux waves which can induce electromotive forces (EMF) in stator coils are those that have number of pole-pairs equal to the pole-pair number of the space harmonics of the resulting stator MMF.

3. Analytical study of induction motor with dynamic airgap eccentricity

3.1. The stator flux density of symmetrical three-phase stator windings under dynamic eccentricity

The occurrence of DE introduces unequal airgap and therefore modifies the expression of the airgap permeance. Therefore, the stator and the rotor flux densities must be recalculated. The task then is to formulate analytical expression for the airgap permeance in the case of DE.

Fig. 3 represents an induction machine, with a smooth airgap, supported in its bearings eccentrically with respect to the stator. The rotor centre is shifted by a distance a from the stator centre. It should be noticed that we consider only the type of eccentricity where the axis of the rotor is parallel to the stator axis. In this case, if r and R denote the rotor and stator radius, respectively, the airgap length δ can be written as

$$\delta = R - r - a\cdot\cos\alpha = \delta_0 - a\cdot\cos\alpha \quad (19)$$

With $\delta_0 = R - r$ is the mean airgap length when the rotor is perfectly centred in the stator bore. In the case of DE, the angle α is a function of the angular displacement θ and time t as follows:

$$\alpha = \omega_r t - \theta \quad (20)$$

where $\omega_r = \omega_s(1-s)/p$ is the mechanical rotational pulsation.

Consequently, the airgap length (referenced to stator) can be written as

$$\delta(t,\theta) = \delta_0 - a\cdot\cos(\omega_r t - \theta) = \delta_0[1 - \varepsilon\cos(\omega_r t - \theta)] \quad (21)$$

With $\varepsilon = a/\delta_0$ the relative eccentricity. Therefore, the airgap permeance is given by

$$P_{de}(t,\theta) = \frac{\mu_0}{\delta(t,\theta)} = \frac{\mu_0}{\delta_0[1 - \varepsilon\cos(\omega_r t - \theta)]} \quad (22)$$

The airgap permeance can be resolved in a Fourier series as follows:

$$P_{de}(t,\theta) = P_0 + \sum_{n=1}^{\infty} P_n\cos n(\omega_r t - \theta) \quad (23)$$

with n an integer represents the order of the permeance harmonics, $P_0 = \frac{1}{\delta_0\sqrt{1-\varepsilon^2}}$ and $P_n = 2P_0\cdot\left(\frac{1-\sqrt{1-\varepsilon^2}}{\varepsilon}\right)^n$.

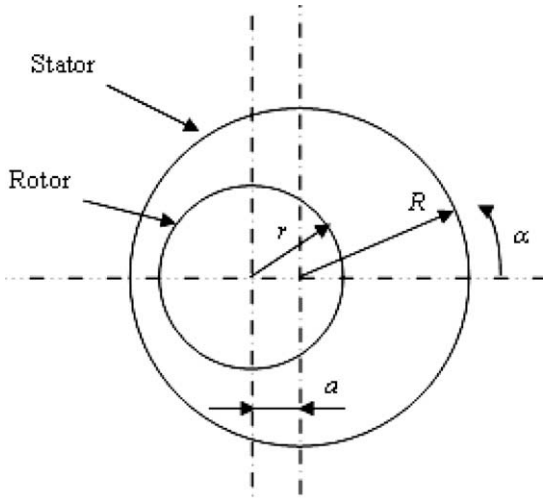

Fig. 3. Eccentrically supported rotor.

Expression (23) shows that the airgap permeance has a constant term and infinite series of harmonics due to DE. For a small values of relative eccentricity ($\varepsilon \ll 1$), the airgap permeance can be restricted to the first harmonic [14,21]. But, in this study, all the permeance harmonics are considered.

Since the stator windings structure is not affected by DE, the stator MMF is still the same as in the healthy state (4). Consequently, the stator flux density (in the case of DE) is obtained by multiplying the permeance function (23) with the stator MMF (4). Hence, one can obtain (with respect to the stator):

$$\begin{aligned} B_{sh}^{P_{de}}(t,\theta) &= \widehat{B}_{sh}^{P_0}\cos(\omega_s t \pm hp\theta) \\ &+\widehat{B}_{sh}^{P_n}\cos[(\omega_s \mp n\omega_r)t - (hp \mp n)\theta] + \widehat{B}_{sh}^{P_n}\cos[((\omega_s \mp n\omega_r)t + (hp \pm n)\theta)] \end{aligned} \tag{24}$$

It is clear, from (24), that DE produces new stator flux density components at $(f_s \pm nf_r)$ Hz with corresponding $(hp \pm n)$ pole-pairs.

3.2. The rotor flux density under dynamic eccentricity

The stator flux density harmonics of expression (24) will induce EMFs into the rotor cage, hence generating circulating rotor currents. In tern, these rotor currents produce rotor MMF waves with further components. So, the general term of the rotor MMF, in the case of DE, can be expressed as (rotor referenced):

$$\begin{aligned} F_{rh}^{P_{de}}(t,\theta_r) &= \widehat{F}_{rh}^{P_0}\cos(s_h\omega_s t \pm hp\theta_r) + \widehat{F}_{rhSH1,2}^{P_0}\cos[s_h\omega_s t \pm (kN_r \mp hp)\theta_r] + \widehat{F}_{rhn}^{P_n}\cos[s_h\omega_s t \pm (hp \pm n)\theta_r] \\ &+ \widehat{F}_{rhnSH1,2}^{P_n}\cos[s_h\omega_s t \pm (kN_r \mp (hp \pm n))\theta_r] \end{aligned} \tag{25}$$

The interaction of the above expression with the eccentric airgap permeance function represented by (23) gives the rotor flux density. But note that (23) must be expressed in a rotor reference frame as follows:

$$P_{de}(t,\theta_r) = P_0 + \sum_{n=1}^{\infty} P_n \cos n(\theta_r) \tag{26}$$

Consequently, the general term of the rotor flux density waves, can be written as:

$$\begin{aligned} B_{rh}^{P_{de}}(t,\theta_r) &= \widehat{B}_{rh}^{P_0,P_0}\cos(s_h\omega_s t \pm hp\theta_r) + \widehat{B}_{rhSH1,2}^{P_0,P_0}\cos[s_h\omega_s t \pm (kN_r \mp hp)\theta_r] + \widehat{B}_{rhn}^{P_n,P_0}\cos[s_h\omega_s t \pm (hp \pm n)\theta_r] \\ &+ \widehat{B}_{rhnSH1,2}^{P_n,P_0}\cos[s_h\omega_s t \pm (kN_r \mp (hp \pm n))\theta_r] + \widehat{B}_{rhn}^{P_n,P_n}\cos[s_h\omega_s t \pm (hp \pm n \pm n)\theta_r] \\ &+ \widehat{B}_{rhnSH1,2}^{P_n,P_n}\cos[s_h\omega_s t \pm (kN_r \mp (hp \pm n \pm n))\theta_r] \end{aligned} \tag{27}$$

One can observe the presence of new rotor flux density components with $(hp \pm n)$ and $(hp \pm n \pm n)$ pole-pair numbers. It is clear that $(\pm n \pm n)$ can be equal to: $-2n$, 0 or $+2n$. To observe (27) from the stator side, we use the transformation given by (16). Hence, one can obtain:

$$\begin{aligned} B_{rh}^{P_{de}}(t,\theta) &= \widehat{B}_{rh}^{P_0,P_0}\cos(\omega_s t \pm hp\theta) \\ &+ \widehat{B}_{rhSH1,2}^{P_0,P_0}\cos[(1 \mp kN_r(1-s)/p)\omega_s t \pm (kN_r \mp hp)\theta] \\ &+ \widehat{B}_{rhn}^{P_n,P_0}\cos[(1 \pm n(1-s)/p)\omega_s t \pm (hp \pm n)\theta] \\ &+ \widehat{B}_{rhnSH1,2}^{P_n,P_0}\cos[(1 \mp (kN_r \pm n)(1-s)/p)\omega_s t \pm (kN_r \mp (hp \pm n))\theta] \\ &+ \widehat{B}_{rhn}^{P_n,P_n}\cos\left[\left(1 \pm \left(\underbrace{\pm n \pm n}_{A}\right)(1-s)/p\right)\omega_s t \pm \left(hp\underbrace{\pm n \pm n}_{B}\right)\theta\right] \\ &+ \widehat{B}_{rhnSH1,2}^{P_n,P_n}\cos\left[\left(1 \mp \left(kN_r\underbrace{\pm n \pm n}_{A}\right)(1-s)/p\right)\omega_s t \pm \left(kN_r \mp \left(hp\underbrace{\pm n \pm n}_{B}\right)\right)\theta\right] \end{aligned} \tag{28}$$

The above expression shows that the rotor flux density encloses a variety of waves with different frequencies and pole-pair numbers. So, they must be analysed carefully, in order to identify which waves can induce EMF into the stator windings. From (28), one can note that the first two waves are due the interactions between the harmonics of (25) containing the P_0 term, and the constant part of the airgap permeance of (26). Since these waves have (hp) and $(kN_r \pm hp)$ pair of poles, they can induce EMF in the stator windings even the motor is in healthy state as it mentioned previously.

The second two waves of (28) are due to the interactions between the harmonics of (25) containing the P_0 term and the eccentric part of permeance function in (26). These waves are also produced by the interactions between the constant part of (26) and the harmonics of (25) having the P_n term. It is obvious that these waves have $(hp \pm n)$ and $(kN_r \pm hp \pm n)$ pair of poles which are clearly depended on n that represents the order of the permeance harmonics. Consequently, they can induce EMF in the stator windings if only their pole-pair number belongs to the set $\{hp\}$. As an example, for a motor with 4-poles and 28 rotor bars without neutral connection, we have: $\{hp\} = \{2, 10, 14, 22, \ldots 2 \times (6k \pm 1)\}$. In this case, the second three waves cannot induce EMF in the stator windings for all n, but only for $n = 8, 12, 20, 24, 32, 36, \ldots$

Finally, the last two waves of (28) are purely generated by the interactions between harmonics of (25) and (26) that contain the P_n term. As can be clearly seen, these waves have $\left(hp\underbrace{\pm n \pm n}_{B}\right)$ and $\left(kN_r \pm hp\underbrace{\pm n \pm n}_{B}\right)$ pair of poles which are obvi-

ously depended on $(\pm n \pm n)$. The corresponding frequencies of these waves are given by: $\left(f_s \pm \underbrace{(\pm n \pm n)}_{A} f_r\right)$ Hz and $\left(f_{RSH} \pm \underbrace{(\pm n \pm n)}_{A} f_r\right)$ Hz. The terms A and B can be equal to: $-2n$, 0 or $+2n$, and it is so important to know that all combinations between A and B are possible. As a result, it is possible to find rotor airgap flux density waves at $(f_s \pm 2nf_r)$ Hz and $(f_{RSH} \pm 2nf_r)$ Hz with corresponding (hp) and $(kN_r \pm hp)$ pole-pairs respectively, which belong to the set $\{hp\}$ and therefore, they induce EMF into the stator windings.

In the light of this analysis, one can state that, due to the dynamic airgap eccentricity, specific components appear in the stator current spectra, around the fundamental and the PSH, at frequencies given by the two following expressions:

$$f_{de1} = |f_s \pm n_{de} f_r| \tag{29}$$

$$f_{de2} = |f_s \pm (N_r \pm n_{de}) f_r| \tag{30}$$

with $n_{ed} = 2, 4, 6 \ldots$

Since in practice, the power supply is not purely sinusoidal, currents in phases are also not purely sinusoidal, but contain time harmonics. Taking into account these harmonics, the expressions (29) and (30) can be written, respectively, as follows:

$$f_{de1} = |\nu f_s \pm n_{de} f_r| \tag{31}$$

$$f_{de2} = |\nu f_s \pm (N_r \pm n_{de}) f_r| \tag{32}$$

where $\nu = 1, 3, 5, \ldots$ is the order of the time supply harmonics.

4. Simulation results

It is important to note that in practice, induction motors are not perfectly symmetrical. Even in healthy state, they have some inherent levels of static and dynamic airgap eccentricities. This means that until now, the DE can not be studied experimentally separately from the SE. Consequently, only simulation, based on accurate mathematical models, can provide useful information about the behaviour of the induction motors under DE condition, and then enables us to identify the line components that are only a function of this fault.

4.1. System equations

In this work, the simulation results are obtained from an accurate transient model of squirrel cage induction motors. This model is based on the multiple-coupled circuits [14,16,21]. As it described previously, the rotor cage can be regarded as a whole of meshes connected between them electrically and coupled magnetically which can lead to the following voltage equations:

$$[U_s] = [R_s][I_s] + \frac{\mathrm{d}[\psi_s]}{\mathrm{d}t} \tag{33}$$

$$[0] = [R_r][I_r] + \frac{\mathrm{d}[\psi_r]}{\mathrm{d}t} \tag{34}$$

where

$$[\psi_s] = [L_{ss}][I_s] + [L_{sr}][I_r] \tag{35}$$

$$[\psi_r] = [L_{rs}][I_s] + [L_{rr}][I_r] \tag{36}$$

The equation describing the mechanical part of the system is

$$C_e - C_r = J_r \frac{\mathrm{d}\omega_r}{\mathrm{d}t} \tag{37}$$

with

$$C_e = \left(\frac{\mathrm{d}W_{co}}{\mathrm{d}\theta_r}\right)\Big|_{(I_s, I_r = \text{constant})} \tag{38}$$

and

$$W_{co} = \frac{1}{2}\Big([I_s]^T[L_{ss}][I_s] + [I_s]^T[L_{sr}][I_r] + [I_r]^T[L_{rr}][I_r] + [I_r]^T[L_{rs}][I_s]\Big) \tag{39}$$

where $[U_s]$, stator voltages vector; $[I_s]$,$[I_r]$, stator and rotor currents vectors; $[R_s]$, (3×3) stator resistance matrix; $[L_{ss}]$, (3×3) stator inductance matrix; $[L_{sr}]$, $3 \times (N_r + 1)$ mutual inductance matrix; $[R_r]$, $(N_b + 1) \times (N_b + 1)$ rotor resistance matrix; $[L_{rr}]$, $(N_b + 1) \times (N_b + 1)$ rotor inductance matrix.

4.2. Calculation of inductances

It is well known that a successful simulation of the induction motors requires a precise calculation of all motor inductances. For that reason, the Modified Winding Function Approach (MWFA) has been used for determining the self inductances of stator coils and rotor loops as well as the mutual inductances between them in both healthy and airgap eccentricity conditions. The skewing rotor bars effects and the linear rise of MMF across the slot were also considered thanks to an extension in 2-D of the MWFA. Using this technique, the resulting inductances expressions are less complicated than those obtained starting from the expression of inductance per unit of length. This makes easy their implementation into algorithm and represents a good compromise between the performance of the model and the computation time. For more details, see [15,16,24].

The simulation tests were performed on an 11 kW, 4-poles, 40 rotor bars three-phase induction motor [25]. The stator windings are coupled in star with neutral connection. Initially, the motor inductances were calculated for healthy state then with 50% of DE. Fig. 4 illustrates the effects of DE on the self inductance of the stator phase *A* (Fig. 4a and b) and on the mutual inductance between phase *A* and the first rotor loop *r*1 (Fig. 4c and d).

After that, the motor was simulated in healthy state then with 50% of DE. the Fast Fourier Transform (FFT) was used to explore the spectral contents of the stator line currents. Fig. 5 confirms that, in healthy state, the stator current spectrum includes only the fundamental and the principle slot harmonics (PSH). However, when considering 50% of DE, Figs. 6 and

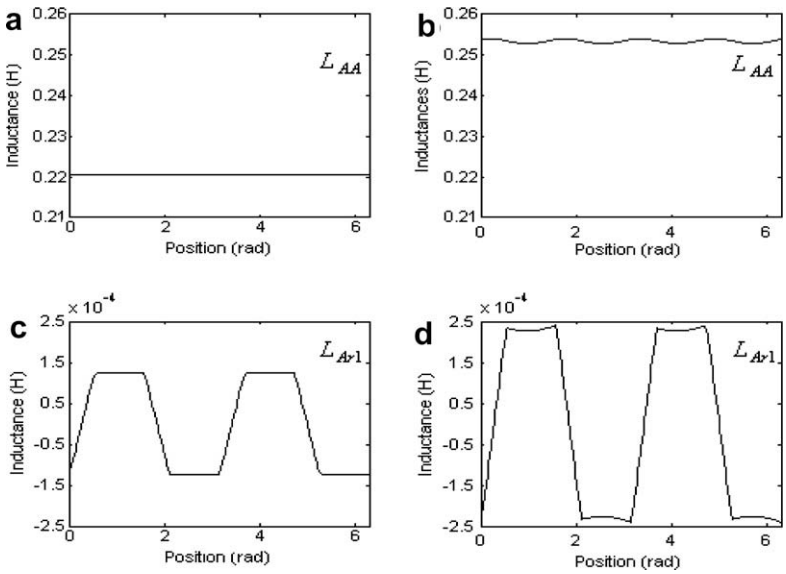

Fig. 4. The effects of DE on the motor inductances. (a) and (c) healthy motor, (b) and (d) 50% of DE.

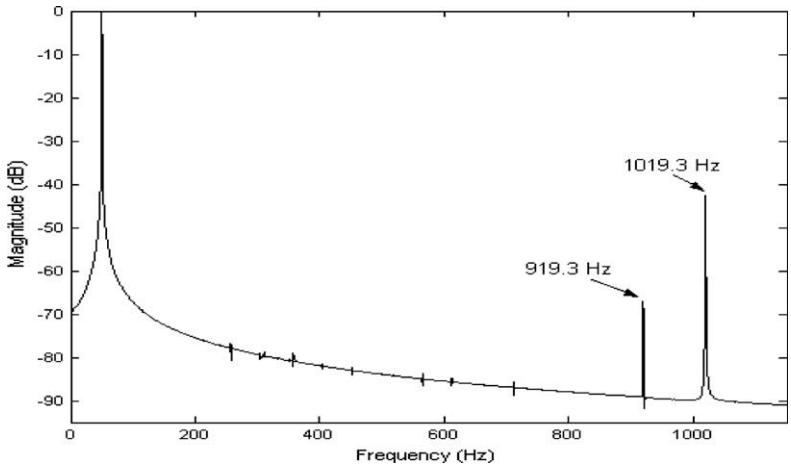

Fig. 5. Stator current spectrum for healthy motor at rated load.

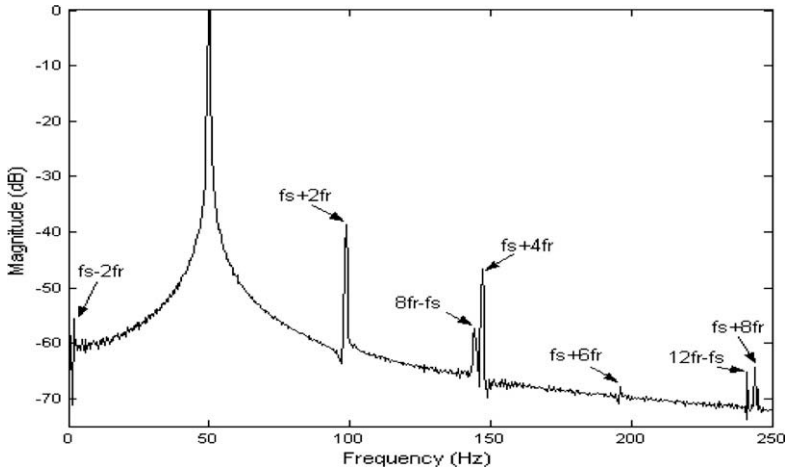

Fig. 6. Stator current spectrum with 50% of DE, $s = 0.0286$ (zoom around the fundamental).

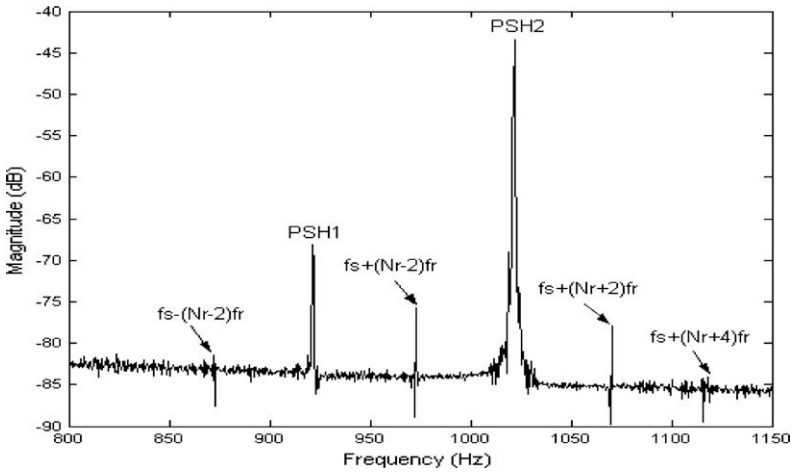

Fig. 7. Stator current spectrum with 50% of DE, $s = 0.0286$ (zoom around the PSH).

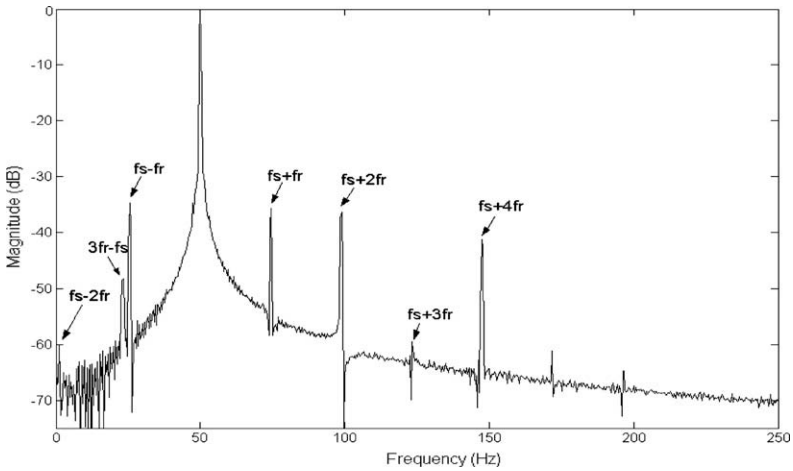

Fig. 8. Stator current spectrum with 5% of SE and 50% of DE, $s = 0.0245$.

7 show clearly the presence of specific frequency components around the fundamental and the PSH. These components are in total agreement with the expressions (29) and (30).

Since the motors are not perfectly symmetrical, the effect of the inherent SE must be illustrated. For that reason, a small level of SE (5%) was introduced in addition to the 50% of DE. Fig. 8 shows clearly that the inherent SE interacts with the DE and gives rise to spectral components which are related to the mixed airgap eccentricity (at frequencies given by expression (2)).

5. Conclusion

In this work, the stator line currents of three-phase squirrel cage induction motor, operating under healthy and with dynamic airgap eccentricity were analysed using the rotating field approach. This study was performed mainly to show the exact signatures of the dynamic airgap eccentricity. It was demonstrated that, theoretically, this fault generates spectral components around the fundamental and the PSH at the frequencies given by the expressions (29) and (30). But, in reality, the induction motors are not perfectly symmetrical; in this direction, it was shown that an inherent level of SE is sufficient to interact with DE and produce therefore, spectral components related to the mixed eccentricity (expression (2)).

Finally, this work can be regarded as an important theoretical study, because it provides analytical explanations to some experimental observations shown in many previous papers and gives answers to some questions about the effect of the DE on the stator current spectra.

Appendix

Rating power	11 kW
Rated frequency	50 Hz
Number of pole-pairs	2
Number of rotor bars	40
Number of stator slots	48
Turns per coil	28
Length of stator stack	0.11 m
Rotor bar resistance	31 μΩ
End ring resistance	2.2 μΩ
Average radius	0.082 m
Air gap length	0.0008 m
Phase resistance	1.75 Ω
Rotor inertia	0.0754 kg m^2

References

[1] S. Nandi, H.A. Toliyat, X. Li, Condition monitoring and fault diagnosis of electrical motors – a review, IEEE Trans. Energy Conver. 20 (4) (2005) 719–729.
[2] A.H. Bonnett, G.C. Soukup, Cause and analysis of stator and rotor failures in three-phase squirrel-cage induction motors, IEEE Trans. Ind. Appl. 28 (4) (1992) 921–937.
[3] D.G. Dorrell, W.T. Thomson, Analysis of airgap flux, current, and vibration signals as a function of the combination of static and dynamic airgap eccentricity in 3-phase induction motors, IEEE Trans. Ind. Appl. 33 (1) (1997) 24–34.
[4] J.R. Cameron, W.T. Thomson, A.B. Dow, Vibration and current monitoring for detecting airgap eccentricity in large induction motors, Proc. IEE 33 (3) (1986) 55–163.
[5] J. Penman, M.N. Dey, A.J. Tait, W.E. Bryan, Condition monitoring of electrical drives, Proc. IEE 133 (3) (1986) 42–148.
[6] Z. Liu, X. Yin, Z. Zhang, D. Chen, W. Chen, Online rotor mixed fault diagnosis way based on spectrum analysis of instantaneous power in squirrel cage induction motors, IEEE Trans. Energy Conver. 19 (3) (2004) 483–490.
[7] W.T. Thomson, M. Fenger, Current signature analysis to detect induction motor faults, IEEE Mag. Ind. Appl. 7 (4) (2001) 26–34.
[8] J.A. Daviua, P. Joverb, M. Rieraa, A. Arkkiob, J.R. Folch, DWT analysis of numerical and experimental data for the diagnosis of dynamic eccentricities in induction motors, Mech. Syst. Signal Process. (2007), doi:10.1016/j.ymssp.2007.01.008.
[9] G.B. Kliman, J. Stein, Methods of motor current signature analysis, Electr. Mach. Power Syst. 20 (5) (1992) 463–474.
[10] M.E.H. Benbouzid, A review of induction motors signature analysis as a medium for faults detection, IEEE Trans. Ind. Electr. 47 (5) (2000) 984–993.
[11] W.T. Thomson, D. Rankin, D.G. Dorrell, On line current monitoring to diagnose airgap eccentricity in large three-phase induction motors – industrial case histories verify the predictions, IEEE Trans. Energy Conver. 14 (4) (1999) 372–1378.
[12] S. Nandi, S. Ahmed, H.A. Toliyat, Detection of rotor slot and other eccentricity related harmonics in a three phase induction motor with different rotor cages, IEEE Trans. Energy Conver. 16 (3) (2001) 253–260.
[13] W.T. Thomson, A. Barbour, C. Tassoni, F. Filippetti, An appraisal of the MMF-permeance method and finite element models to study static airgap eccentricity and its diagnosis in induction machines, in: Proc. ICEM'98 Conf., Istanbul, Turkey, pp. 2182–2187.
[14] S. Nandi, R.M. Bharadwaj, H.A. Toliyat, Performance analysis of three-phase induction motor under mixed eccentricity condition, IEEE Trans. Energy Conver. 17 (3) (2002) 392–399.
[15] A. Ghoggal, Diagnostic de la machine asynchrone triphasée: modèle dédié à la détection des défauts, Magistere thesis, Dept. of Elec. Eng. University of Batna, Algeria, May 2005.
[16] A. Ghoggal, A. Aboubou, S.E. Zouzou, M. Sahraoui, H. Razik, Considerations about the modelling and simulation of air-gap eccentricity in induction motors, in: IEEE IECON Conf., Paris, France, 2006, pp. 4987–4992.

[17] A. Knight, S.P. Bertani, Mechanical fault detection in a medium-sized induction motor using stator current monitoring, IEEE Trans. Energy Conver. 20 (4) (2005) 753–760.
[18] B. Heller, V. Hamata, Harmonic Field Effects in Induction Machines, Elsevier Scientific Publishing Co., Prague, 1977.
[19] A.J.M. Cardoso, E.S. Saraiva, Computer-aided detection of airgap eccentricity in operating three-phase induction motors by Park's vector approach, IEEE Trans. Ind. Appl. 29 (5) (1993) 897–901.
[20] J. Faiz, B.M. Ebrahimi, H.A. Toliyat, B. Akin, Diagnosis of a mixed eccentricity fault in a squirrel-cage three-phase induction motor using time stepping finite element technique, in: Proc. IEEE IEMDC Conf., vol. 2, 2007, pp. 1446–1450.
[21] G. Joksimovic, M. Djurovic, J. Penman, N. Arthur, Dynamic simulation of dynamic eccentricity in induction machines – winding function approach, IEEE Trans. Energy Conver. 5 (2) (2000) 143–148.
[22] X. Li, Q. Wu, S. Nandi, Performance analysis of a three-phase induction machine with inclined static eccentricity, IEEE Trans. Ind. Appl. 43 (2) (2007) 531–541.
[23] M. Drif, A.J.M. Cardoso, The use of instantaneous phase-angle signature analysis for airgap eccentricity diagnosis in three-phase induction motors, in: Proc. POWERENG, Conf., Setubal, Portugal, April 2007, pp. 100–105.
[24] A. Ghoggal, M. Sahraoui, A. Aboubou, S.E. Zouzou, H. Razik, An improved model of the induction machine dedicated to faults-detection – extension of the modified winding function, in: Proc. IEEE ICIT Conf., Hong-Kong, China, 2005, pp.191–196.
[25] G. Joksimovic, Dynamic simulation of cage induction machine with air gap eccentricity, IEE Proc. Electr. Power Appl. 152 (4) (2005) 803–810.
[26] X. Huang, T.G. Habetler, R.G. Harley, Detection of rotor eccentricity faults in a closed-loop drive-connected induction motor using an artificial neural network, IEEE Trans. Power Electr. 22 (4) (2007) 552–1559.
[27] X. Huang, T.G. Habetler, R.G. Harley, Using a surge tester to detect rotor eccentricity faults in induction motors, IEEE Trans. Ind. Appl. 43 (5) (2007) 1183–1190.
[28] J. Grieger, R. Supangat, N. Ertugrul, W.L. Soong, D.A. Gray, C. Hansen, Estimation of static eccentricity severity in induction motors for on-line condition monitoring, in: Proc. IEEE IAS Conf., Tampa, USA, 2006, pp. 2312–2319.
[29] H. Su, K.T. Chong, Induction machine condition monitoring using neural network modelling, IEEE Trans. Ind. Electr. 54 (1) (2007) 241–249.
[30] S. Bachir, S. Tnani, C.C. Trigeassou, G. Champenois, Diagnosis by parameter estimation of stator and rotor occurring in induction machines, IEEE Trans. Ind. Electr. 53 (3) (2006) 963–973.
[31] I.M. Culbert, W. Rhodes, Using current signature analysis technology to reliably detect cage winding defects in squirrel-cage induction motors, IEEE Trans. Ind. Appl. 43 (2) (2007) 422–428.
[32] J.H. Jung, J.J. Lee, B.H. Kwon, Online diagnosis of induction motors using MCSA, IEEE Trans. Ind. Electr. 53 (6) (2006) 1842–1852.
[33] H. Guldemir, Detection of airgap eccentricity using lines current spectrum of induction motors, Electr. Power Syst. Res. 64 (2003) 109–117.
[34] G.G. Acosta, C.J. Verucchi, E.R. Gelso, A current monitoring system for diagnosing electrical failures in induction motors, Mech. Syst. Signal Process. 20 (2006) 953–965.
[35] G.K. Snigh, S.A. S Al Kazzaz, Induction machine drive condition monitoring and diagnostic research – a survey, Electr. Power Syst. Res. 64 (2003) 145–158.